ACS APPLIED MATERIALS & INTERFACES

Research Article

www.acsami.org

Improvement in Half-Life of Organic Solar Cells by Using a Blended Hole Extraction Layer Consisting of PEDOT:PSS and Conjugated Polymer Electrolyte

Eui Jin Lee, Jae Pil Han, Seung Eun Jung, Min Hee Choi, and Doo Kyung Moon*

Department of Materials Chemistry and Engineering, Konkuk University, 120, Neungdong-ro, Gwangjin-gu, Seoul 05029, Korea

Supporting Information

ABSTRACT: In this study, we fabricated conventional structured organic solar cells (OSCs) by introducing a hole extraction layer (HEL) that consisted of poly(3,4-ethylenedioxythiophene):polystyrenesulfonate (PEDOT:PSS) and conjugated polymer electrolyte (CPE) poly[9,9-bis(4′-sulfonatobutyl)fluorene-*alt*-thiophene] (PFT-D). PFT-D has a $-SO_3^-$ functional group that acts as a conjugate base against the $-SO_3H$ of PSS. In addition, the molecular dipole of PFT-D can screen the Coulombic attraction between PEDOT chains and PSS chains. By blending PEDOT:PSS and PFT-D, the acidity of the HEL solution and changes to the surface morphology and potential of the HEL film as a function of exposure time in air were reduced. As a result, the half-life of the OSC fabricated with blended HEL was five times better at room temperature and 40% humidity without encapsulation as compared to the pristine PEDOT:PSS-based device.

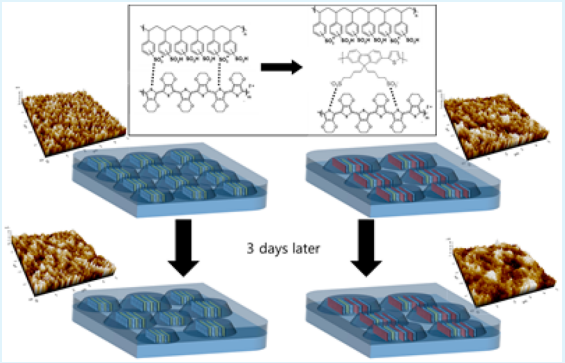

KEYWORDS: *organic solar cell, stability, hole extraction layer, conjugated polymer electrolytes, morphological stability, surface potential, phase separation*

Downloaded via KONKUK UNIV on December 4, 2018 at 03:01:31 (UTC).
See https://pubs.acs.org/sharingguidelines for options on how to legitimately share published articles.

INTRODUCTION

Organic solar cells (OSCs) are devices in which a low-cost technology is implemented for producing large-area and lightweight flexible solar modules. In particular, they are regarded as clean and renewable energy devices for next-generation portable, wearable, and building-integrated applications.[1,2] Recently, OSCs with power conversion efficiencies (PCEs) of more than 10%, which makes commercialization of such devices possible, have been reported.[3−5] Thus, the long-term stability of OSCs resulting in a 10−10 target (10% PCE and 10 years of stability) has been spotlighted as an important issue.[6,7]

The photoactive layer (PAL) of OSCs consists of a bulk heterojunction (BHJ) structure comprising a blend of donor and acceptor materials. Excitons formed in the PAL by light are separated into holes and electrons at the interface of the donor and acceptor. The separated charge carriers generate a current by moving into the anode and cathode individually through the highest occupied molecular orbital (HOMO) level of the donor material and the lowest unoccupied molecular orbital (LUMO) level of the acceptor material. However, energy barriers that form between the PAL and the electrodes prevent the transport of charge carriers. In order to solve the energy-level mismatch and improve the PCE of OSCs, interfacial layers are introduced between the PAL and the electrodes.[8−10] These electron- and hole-extracting layers (EELs and HELs, respectively) are drawing attention as important materials in interface engineering.[7,11] The introduction of EELs and HELs greatly contributes not only to the PCE of OSCs but also to improved device stability.

Zirconium acetylacetonate (ZrAcac),[9] cesium carbonate (Cs_2CO_3),[12] and conjugated organic materials such as poly[(9,9-bis(3′-(*N*,*N*-dimethylamino)propyl)-2,7-fluorene)-alt-2,7-(9,9-dioctylfluorene)] (PFN),[13] 3,3′,3″,3‴-((pyrene-1,3,6,8-tetrayltetrakis(benzene-4,1-diyl))tetrakis(oxy))tetrakis(*N*,*N*-dimethylpropan-1-amine) (PBPA),[14] 3,6-bis(5-(4-(3-(dimethylamino)propoxy)phenyl)thiophen-2-yl)-2,5-bis(2-hexyldecyl)pyrrolo[3,4-*c*]pyrrole-1,4(2*H*,5*H*)-dione (DPPA),[15] etc., are used as EEL materials. π-Conjugated polymers such as poly(3,4-ethylenedioxythiophene):polystyrenesulfonate (PEDOT:PSS), conjugated polymer electrolytes (CPEs), and transition metal oxides such as molybdenum oxide (MoO_x),[16] nickel oxide (NiO_x),[17] tungsten oxide (WO_3),[10] etc., have been reported as HEL materials.[7,18−21] PEDOT:PSS is widely used as the hole-transporting material of OLEDs, OSCs, and thin-film solar cells and as a transparent electrode material not only because of its solution processability but also because of its excellent electrical and optical properties.[7,18−22] However, PEDOT:PSS reduces the lifetime of devices by its acidic and hygroscopic properties.[7] In order to offset the drawbacks of

Received: August 6, 2016
Accepted: October 21, 2016
Published: October 21, 2016

© 2016 American Chemical Society

DOI: 10.1021/acsami.6b09846
ACS Appl. Mater. Interfaces 2016, 8, 31791−31798

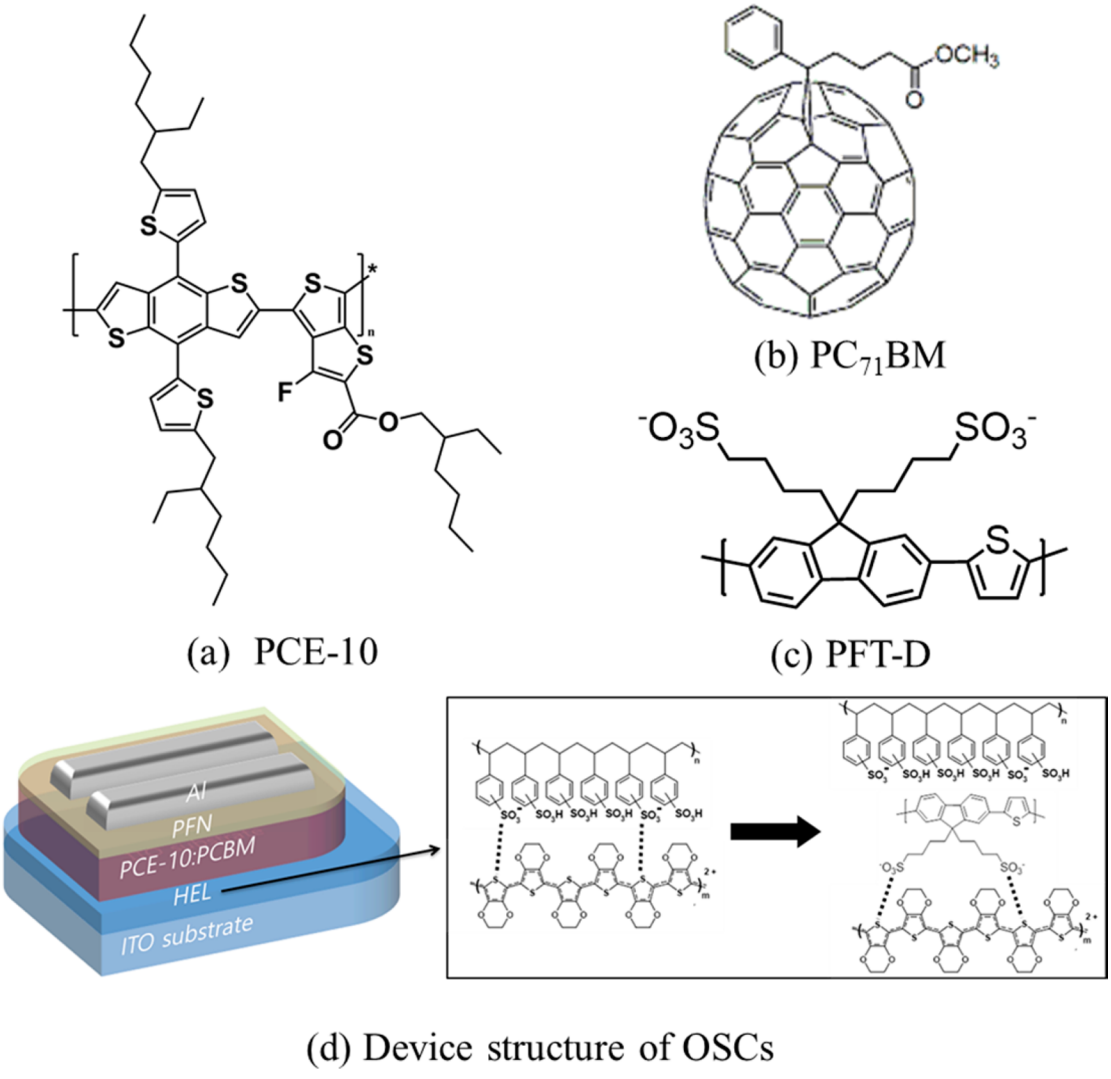

Figure 1. Chemical structures of (a) PCE-10, (b) $PC_{71}BM$, and (c) PFT-D and (d) device structure of the OSCs.

PEDOT:PSS, studies on additives to PEDOT:PSS solutions have been reported.[23−25]

Kim et al. reported the results of a study in which sodium hydroxide, which is a strong base, was added to a PEDOT:PSS solution for the purpose of reducing its acidity. However, as the amount of added NaOH was increased, the performance of the OSC decreased.[23] Ouyang et al. reported the fabrication of a next-generation transparent electrode by improving the conductivity of PEDOT:PSS by proton transfer through the addition of a weak organic acid.[24] Kim et al. reduced the acidity and hygroscopic property of PEDOT:PSS through a condensation reaction with PSS by adding poly(ethylene glycol) methyl ether (PEGME). As a result, they reported that the PCE of the device improved by 21% and that the half-life of the device improved 3.5 times as compared to a pristine PEDOT:PSS-based OSC.[25] In addition, Cao et al. reported that corrosion of ITO and diffusion of indium were reduced by treating neutral PEDOT:PSS with UV-ozone and an oxygen plasma. Consequently, the PCE of the devices with neutral PEDOT:PSS decreases by only 20% after 50 days.[26] However, despite many studies on the improved performance and stability of OSCs through PEDOT:PSS modification, there is insufficient research on the relationship between the changes in the surface properties of the interfacial layer and the lifetime of OSC devices.

Recently, we synthesized a poly[9,9-bis(4′-sulfonatobutyl)-fluorene-*alt*-thiophene] (PFT) CPE and applied it as an HEL to an OSC device.[27] PFT, which is neutral with a pH of 6.7−7.0 and whose dipole moment is used to tune the work function of ITO electrode into 4.95 eV, is a suitable material for hole transporting/extracting. However, the OSC device with the PFT HEL showed a somewhat lower PCE value than the PEDOT:PSS-based device because its work function was slightly lower than that of PEDOT:PSS (5 eV).

In this study, a PFT CPE was modified to a PFT-D CPE by using a $Na_2S_2O_8$ oxidant, and various concentrations of PFT-D were added to PEDOT:PSS. To improve the conductivity and stability of the PEDOT:PSS film, a molecular dipole in PFT-D can be generated between the conjugated backbone and $-SO_3^-$ functional group of the side chain by removing sodium ions[28,29] to screen the Coulombic attraction between PEDOT and PSS through association with PEDOT.[30] We improved the long-term stability without changing the efficiency of the OSC devices by changing the surface morphology and potential of the HEL via the PFT-D additives. Furthermore, we identified the effects of the stability of the HEL morphology and surface potential on the lifetime of the OSC devices. It was concluded

DOI: 10.1021/acsami.6b09846
ACS Appl. Mater. Interfaces 2016, 8, 31791−31798

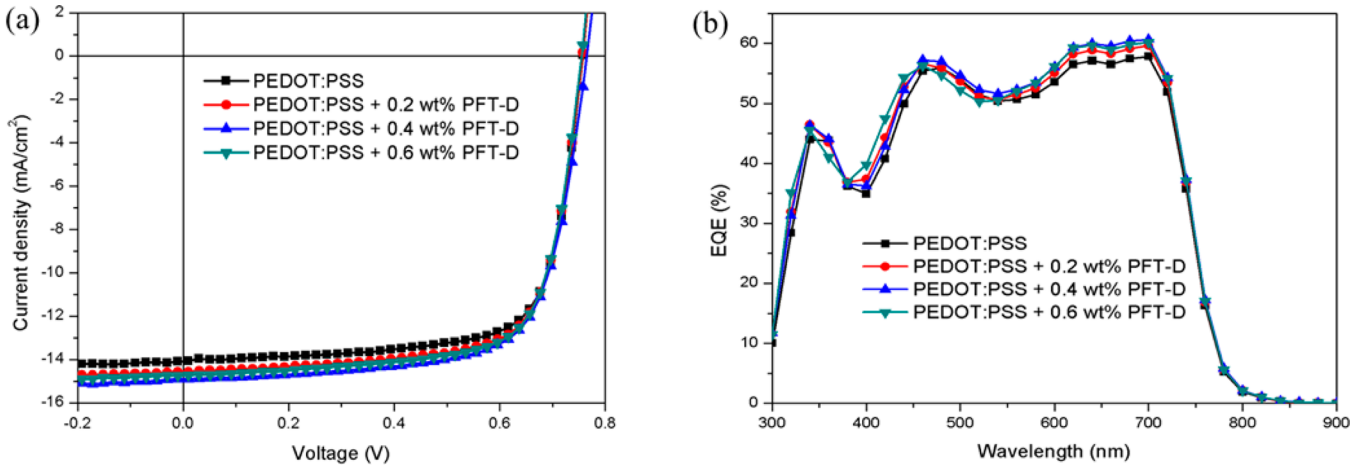

Figure 2. (a) $J-V$ characteristics and (b) EQE characteristics of OSCs.

Table 1. Device Performance Parameters of the OSCs[a]

PFT-D concentration	V_{oc} [V]	J_{sc} [mA/cm^2]	FF [%]	PCE [%]	R_{sh} [Ω cm^2]
0 wt %	0.76 (0.76)	14.1 (14.20)	72.8 (71.85)	7.8 (7.75)	523
0.2 wt %	0.76 (0.76)	14.6 (14.57)	71.8 (71.50)	8.0 (7.92)	959
0.4 wt %	0.77 (077)	14.9 (14.67)	71.3 (71.23)	8.2 (8.04)	1190
0.6 wt %	0.76 (0.76)	14.7 (14.72)	71.5 (70.93)	8.0 (7.94)	1010

[a]The values in the parentheses represent the average values of four cells.

that the changes in the morphology and surface potential of the HEL surface decreased as a function of the time and that the stability of the OSC devices increased more than five times.

EXPERIMENTAL SECTION

Fabrication of OSC Devices. To fabricate the OSC devices, patterned ITO glass substrates were washed by sonication in detergent, 2-propanol, and deionized water in sequence. After cleaning, the ITO glass substrates were dried at 120 °C and UV–ozone treated for 15 min. For the HEL solution, PFT-D in concentrations of 0, 0.2, 0.4, and 0.6 wt % was added to PEDOT:PSS (Heraeus, P VP AI 4083). The solutions were filtered through a 0.45 μm PTFE filter and spin coated onto the ITO glass substrates and annealed at 140 °C (0 wt %) or 120 °C (0.2, 0.4, and 0.6 wt %) for 10 min to form HELs with thicknesses of 30 nm. Solutions with a PFT-D concentration greater than 0.6 wt % were not filtered through the 0.45 μm PTFE filter (Figure S1, Supporting Information). When the solutions were coated without filtering, the surface of the HELs was not uniform, which can affect the reliability of the devices. The prepared samples were then transferred to a N_2-filled glovebox, and poly[4,8-bis(5-(2-ethylhexyl)thiophen-2-yl)benzo[1,2-b;4,5-b′]-dithiophene-2,6-diyl-*alt*-(4-(2-ethylhexyl)-3-fluorothieno[3,4-*b*]-thiophene)-2-carboxylate-2–6-diyl] (PCE-10, 1-materials) and [6,6]-phenyl C_{71} butyric acid methyl ester ($PC_{71}BM$) (1:1.5, w/w) in chlorobenzene/1,8-diiodooctane (97:3, v/v) solution were spin coated onto the samples to form photoactive layers with thicknesses of 80 nm. To form an electron extraction layer, a PFN solution (2 mg/mL in methanol with 2 μL/mL of acetic acid) was spin coated onto the photoactive layer of the samples. Finally, an Al cathode (100 nm) was thermally deposited in a high vacuum chamber (<10^{-7} Torr). The active area of the fabricated OSCs was 7 mm^2.

Measurements. The thicknesses of the prepared thin films were measured using an Alpha Step 500 surface profiler (KLA-Tencor) and atomic force microscopy (AFM, psia XE-100, contact mode). The optical transmittance of the HELs and the light absorption of PCE-10 were characterized using an ultraviolet–visible (UV–vis) spectrometer (Agilent 8453). The sheet resistances of the ITO electrode were measured by using a four-point probe station (MST 6000C). The surface morphologies and potentials of the HELs were characterized by AFM (psia XE-100, noncontact mode) and external electrostatic force microscopy (EFM). The work function of the ITO/HELs was measured by scanning Kelvin probe microscopy. X-ray photoelectron spectroscopy (XPS, PHI 5000 Versa Probe II) was used to investigate the surface composition of the HELs. The current density–voltage ($J-V$) characteristics of the fabricated OSCs were assessed using a Keithley 2400 source measurement unit and an AM 1.5G solar simulator (Oriel 96000 150 W solar simulator). The incident photon-to-current conversion (IPCE) was measured to determine the best performance of the devices.

RESULTS AND DISCUSSION

Figure 1 shows the molecular structure of PCE-10, $PC_{71}BM$, and PFT-D and the device structure of the fabricated OSCs. OSCs with conventional structures were fabricated as shown in Figure 1(d).

The device performance of the OSCs is presented in Figure 2 and summarized in Table 1. In Figure S3 and Table S1, the device performance of OSC devices based on the PTB7:$PC_{71}BM$ system is also shown. The OSC device with PEDOT:PSS showed a maximum PCE of 7.8%, with an open-circuit voltage (V_{OC}) of 0.76 V, a short-circuit current density (J_{SC}) of 14.1 mA/cm^2, and a fill factor (FF) of 72.8%. On the other hand, when 0.2 wt % PFT-D was added to PEDOT:PSS, a V_{OC} of 0.77 V, a J_{SC} of 14.9 mA/cm^2, and a FF of 71.3% were obtained, resulting in a PCE of up to 8.2%. This PCE improvement was mainly because of increased J_{SC} caused by the addition of PFT-D. As can be seen in Figure S2 and Figure S4 (Supporting Information), the higher PCE is a result of the increased current generation by the absorption of more light in the PAL, which itself was the result of the enhanced optical transmittance in the 560–750 nm wavelength range corresponding to the main absorption band of PCE-10 and of improved charge carrier extraction from the PAL to the external circuit. Values for the PL quenching rate were calculated from the difference between the area of the PL spectrum of PCE-10

DOI: 10.1021/acsami.6b09846
ACS Appl. Mater. Interfaces 2016, 8, 31791–31798

only and the BHJ films. As the quenching rate increases, the dissociation and extraction of charge carriers improve.[31−33] As a result, the values of the quenching ratio were 83.3%, 85%, 85.6%, and 84.9% for pristine PEDOT:PSS and PEDOT:PSS with 0.2, 0.4, and 0.6 wt % PFT-D added, respectively. These results were confirmed by the fact that the external quantum efficiency (EQE) was improved in the 560−750 nm wavelength area by adding PFT-D, as shown in the IPCE data of Figure 2(b).

Figure S2 (Supporting Information) shows the light absorbance of PCE-10, used as the donor polymer of the PAL, and the optical transmittance of ITO/HEL as a function of the amount of added PFT-D. PCE-10 mainly absorbed light in the 560−750 nm wavelength range (λ_{max} = 704 nm). The HELs on ITO, where PFT-D (0.2−0.6 wt %) was added to PEDOT:PSS, showed slightly higher transmittance values of more than 560 nm (Table S1, Supporting Information) than the pristine PEDOT:PSS. In particular, at λ_{max} = 704 nm for PCE-10, the optical transmittance values (84.06−84.48%) of the PFT-D-added HELs on ITO were slightly higher than that of pristine PEDOT:PSS on ITO (83.61%). Thus, an increase in the amount of light irradiating the PAL is expected.

The fabricated OSC devices were stored without encapsulation at a constant temperature (25 °C) and humidity (40%) under indoor light (~200 lx). The changes in the PCE of the devices as a function of time for approximately 200 h are presented in Figure 3. As PFT-D was added to PEDOT:PSS,

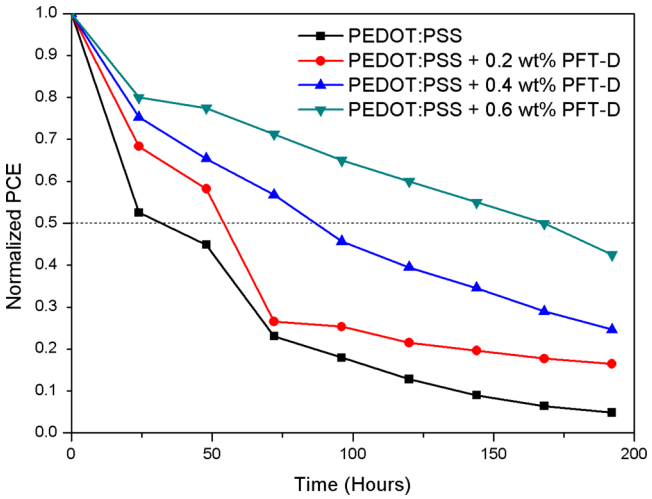

Figure 3. Normalized PCE variation of the devices as a function of time stored in ambient air at 25 °C and 40% humidity under 200 lx interior lighting.

the PCE that was slightly increased now decreased as a function of time. In the case of the device in which pristine PEDOT:PSS was used as the HEL, the PCE rapidly decreased, and the half-life of the device was 32 h. On the other hand, when 0.2, 0.4, and 0.6 wt % PFT-D was added to PEDOT:PSS, the PCE slowly decreased, and the half-lives of the devices were 54, 87, and 168 h, respectively, because of degradation of the J_{sc} and FF of the devices (Figure S5, Supporting Information). The J_{sc} and FF of the devices decreased as a function of time stored in ambient air, whereas V_{oc} was almost constant (Figure S5(b), Supporting Information) because of changes in the electrical conductivity of the ITO electrode and in the surface potential of the HEL film. By introducing HELs in which PFT-D was added to PEDOT:PSS, the half-lives of devices were improved more than five times.

PFT-D is a neutral material with $-SO_3^-$ ions. It can therefore act as a conjugate base for the strongly acidic PSS. The acidity of PEDOT:PSS is due to the ionization of $-SO_3H$, which is the functional group of the PSS polymer chain. The process is represented according to eq 1.

$$-SO_3H \rightleftharpoons H^+ + -SO_3^-,$$
$$K_a = [H^+][-SO_3^-]/[-SO_3H] \quad (1)$$

where K_a is the acid dissociation constant, which represents the ionization equilibrium of $-SO_3H$. Therefore, it always shows a constant value under the same temperature conditions. The equilibrium reaction in eq 1 can be reversed by the addition of PFT-D, so that the pH can be increased as the proton concentration of the solution is decreased.

Figure 4 shows the XPS spectra of the HEL (with both pristine and 0.4 wt % PFT-D added to PEDOT:PSS). Both devices were stored at room temperature (25 °C) with a relative humidity (40%) for 3 days. As shown by the In 3d spectra of the surface of the HELs in Figure 4(a), the amount of indium atoms on the surface of the pristine PEDOT:PSS film dramatically increased due to corrosion of the ITO after 3 days. However, the devices with 0.4 wt % PFT-D added to PEDOT:PSS showed only slightly increased intensity compared to pristine PEDOT:PSS film. The sheet resistance of the ITO with pristine PEDOT:PSS increased from 8.6 to 13.6 Ω/sq. However, devices with PFT-D added showed relatively low sheet resistances of 11.2, 10.4, and 9.8 Ω/sq for 0.2, 0.4, and 0.6 wt % of PFT-D, respectively.

Figures 4(b) and (c) show S 2p XPS spectra of the surface of HELs stored for 10 h and 3 days, respectively. The red solid lines, cyan dots, and purple dots indicate S 2p signals of $-SO_3H$, $-SO_3^-$, and PEDOT, respectively.[34] As can be seen in Figure 4(b), by adding 0.4 wt % PFT-D to PEDOT:PSS, the $-SO_3^-$ peaks decreased, and the $-SO_3H$ peaks increased, compared with a pristine PEDOT:PSS film because of the reverse reaction of eq 1. In other words, the $-SO_3^-$ of PFT-D deactivated the ions of PSS and associated with PEDOT, screening the Coulombic attraction between PEDOT and PSS.[30] In contrast, for pristine PEDOT:PSS, the $-SO_3^-$ peaks increased, and the $-SO_3H$ peaks decreased after 3 days. In this case, the (i) forward reaction of eq 1 and (ii) phase separation of PEDOT:PSS could create PSS-rich regions on the surface of PEDOT:PSS.

Furthermore, the S 2p signals of PSS were confirmed to be more intense than those of PEDOT as shown in Figure 4(b) and (c), suggesting that PSS-rich regions formed on the surface of the PEDOT:PSS film. However, the spectra with 0.4 wt % PFT-D-added PEDOT:PSS did not change very much, compared with that of pristine PEDOT:PSS.

The performance and stability of OSC devices are significantly related to the surface morphology, potential, and stability of the HELs. We therefore measured the surface morphology and potential of the HELs through AFM and EFM. The results are shown in Figure 5 and Figure 6, respectively. Figures 5(a)−(d) show the initial surface morphology of the HELs. In Figure 5(a), the surface of the pristine PEDOT:PSS showed a fine morphology with no aggregation of PEDOT or PSS chains. However, when PFT-D was added, the PEDOT chains aggregated due to separation of the PEDOT and PSS through screening of the Coulombic

DOI: 10.1021/acsami.6b09846
ACS Appl. Mater. Interfaces 2016, 8, 31791−31798

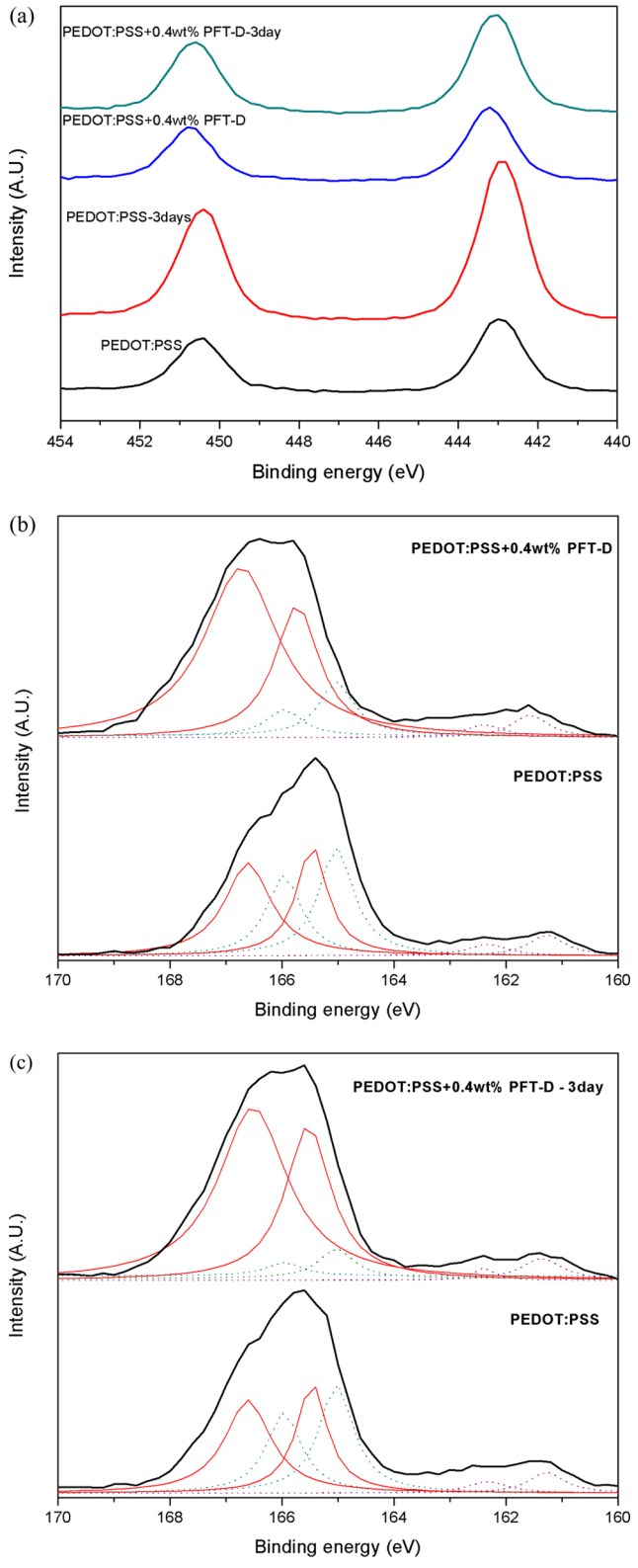

Figure 4. (a) In 3d XPS spectra of pristine and 0.4 wt % PFT-D added PEDOT:PSS and (b), (c) S 2p XPS spectra of pristine and 0.4 wt % PFT-D added PEDOT:PSS after (b) 10 h and (c) 3 days. The red solid lines, cyan dots, and purple dots indicate S 2p signals of $-SO_3H$, $-SO_3^-$, and PEDOT, respectively.

attraction between PEDOT and PSS,[24,30] and smooth, fine films formed on the ITO electrode. As the PFT-D content increased, the value of the root-mean-square roughness (R_{RMS}) increased as a result of the increased grain size. This increase in grain size increased the shunt resistance (R_{sh}) of the OSC devices by improving the conductivity of the HELs (Figure S6, Supporting Information). The conductivity of HELs increased up to the optimal concentration of PFT-D (0.4 wt %) with growth of the PEDOT-rich region. Moreover, when 0.6 wt % PFT-D was added, the conductivity was slightly decreased by the larger PEDOT grains and PSS insulation barrier which caused a longer average distance between the conductive grains.[35,36] By adding PFT-D to PEDOT:PSS, the resistance of the devices decreased compared to the device with pristine PEDOT:PSS HEL.[24,37−39] As a result, the performance of the devices with PFT-D was slightly enhanced.

PEDOT:PSS forms defects due to aggregation caused by moisture in the atmosphere, and the lifetime of devices using PEDOT:PSS can decrease as the defects grow over time.[37] Figure 5(e) shows the surface morphology of pristine PEDOT:PSS after 3 days. In the figure, the aggregation of PEDOT:PSS as compared to Figure 5(a) is confirmed. As a result, the value of R_{RMS} significantly decreased from 1.013 to 0.633 nm.[33,40] On the other hand, in the AFM images of the HELs with PFT-D added [Figures 5(f)−(h)], it is seen that the aggregation of PEDOT:PSS was effectively inhibited as the PFT-D content increased. The changes in the R_{RMS} values were 0.141 and 0.132 nm for PEDOT:PSS HELs with 0.2 and 0.4 wt % PFT-D added, respectively, suggesting that the aggregation of the remaining PEDOT chains, which were associated with PSS chains, was partly inhibited by the addition of 0.2 and 0.4 wt % of PFT-D. However, in the case where 0.6 wt % PFT-D was added [Figures 5(d) and (h)], the change in the R_{RMS} value was 0.028 nm, which means that the effect of the surrounding environment on the surfaces of the HELs was minimized as compared to the pristine PEDOT:PSS (0.381 nm). In contrast, the surface morphology and phase of PALs (Figures S7 and S8, Supporting Information) did not change significantly like the HELs. The R_{RMS} values decreased by only ∼0.1 nm after 3 days, suggesting that a change in the surface of HELs has a more important role than that of PAL in the degradation of devices.

Also, as seen in Figure 6, when PFT-D was added, the surface potential change (ΔSP) of the HELs after 3 days decreased as compared to that of the pristine PEDOT:PSS (ΔSP = 26.22 mV). In the case of the HEL in which 0.6 wt % PFT-D was added, the stability of the OSC was the best, and the ΔSP value was the smallest, 13.77 mV. The surface potential acts as an indicator because it is very sensitive to the electronic states of the surface due to surface charge density or surface traps, surface reconstruction, and chemical composition.[41] PEDOT:PSS forms PSS-rich regions in the upper layer of a film and PEDOT-rich regions in the bottom layer.[42] This vertical phase separation of PEDOT:PSS can be explained by the aggregation of PEDOT chains and the difference in the surface energy between PEDOT chains and PSS chains. Over time, the surface potential could increase because of increasing PSS density on the surface, resulting in aggregation of the PEDOT chains and vertical phase separation. As a result, after 3 days in the case of pristine PEDOT:PSS and PEDOT:PSS doped with 0.2 wt % PFT-D, the surface potential increased by 26.22 and 28.05 mV, respectively. Simultaneously, the J_{sc} of devices with HELs consisting of pristine PEDOT:PSS and PEDOT:PSS doped with 0.2 wt % PFT-D significantly decreased by 9.4 mA/cm^2 (14.1 mA/cm^2 to 4.7 mA/cm^2) and 9.6 mA/cm^2 (14.6 mA/cm^2 to 5.0 mA/cm^2), respectively. However, the changes in J_{sc} of the devices with HELs doped with 0.4 wt % (ΔSP =

DOI: 10.1021/acsami.6b09846
ACS Appl. Mater. Interfaces 2016, 8, 31791−31798

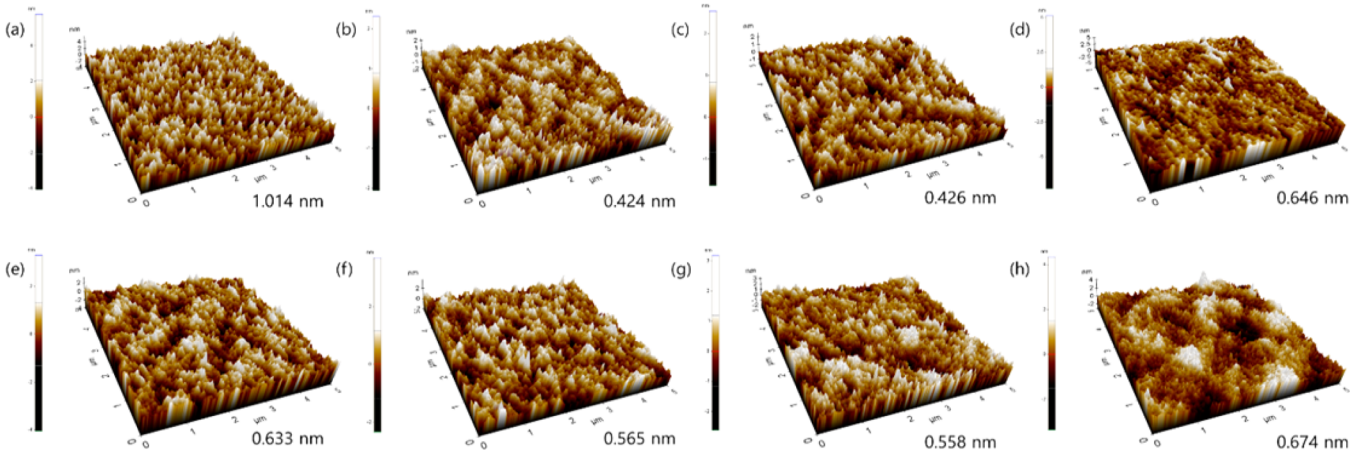

Figure 5. (a)−(d) AFM images of surface morphology of as-cast HELs: (a) PEDOT:PSS, (b) PEDOT:PSS with 0.2 wt % PFT-D, (c) PEDOT:PSS with 0.4 wt % PFT-D, and (d) PEDOT:PSS with 0.6 wt % PFT-D. (e)−(h) AFM images of surface morphology of HELs after 3 days: (e) PEDOT:PSS, (f) PEDOT:PSS with 0.2 wt % PFT-D, (g) PEDOT:PSS with 0.4 wt % PFT-D, and (h) PEDOT:PSS with 0.6 wt % PFT-D.

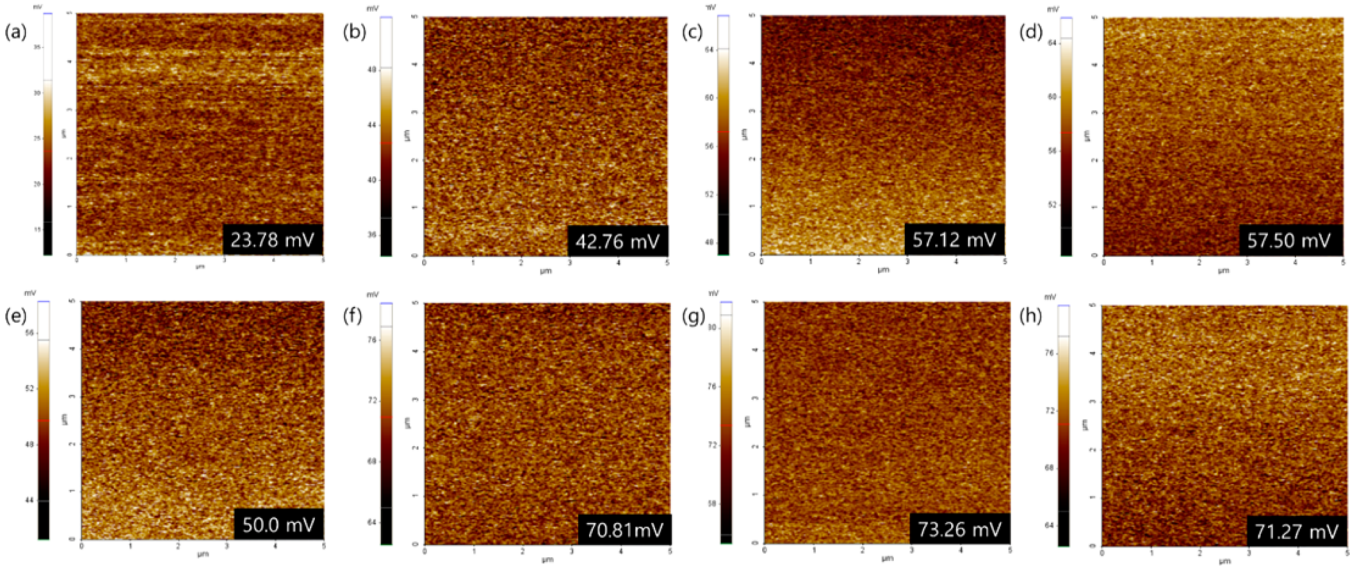

Figure 6. (a)−(d) Surface potentials of as-cast HELs: (a) PEDOT:PSS, (b) PEDOT:PSS with 0.2 wt % PFT-D, (c) PEDOT:PSS with 0.4 wt % PFT-D, and (d) PEDOT:PSS with 0.6 wt % PFT-D. (e)−(h) Surface potentials of HELs after 3 days: (e) PEDOT:PSS, (f) PEDOT:PSS with 0.2 wt % PFT-D, (g) PEDOT:PSS with 0.4 wt % PFT-D, and (h) PEDOT:PSS with 0.6 wt % PFT-D.

16.14 mV) and 0.6 wt % (ΔSP = 13.77 mV) PFT-D were 4.7 mA/cm^2 and 2.5 mA/cm^2, respectively, suggesting that ΔSP are more closely related to ΔJ_{sc} than other factors. On the other hand, the work function of ITO with different HELs had a similar value of about 5 eV (Figure S9, Supporting Information). After 3 days, the work function of the ITO with HELs was slightly higher, and V_{oc} of devices was almost the same. The work function of electrodes is well-known to affect the built-in potential of devices.[42] Therefore, the degradation of devices depends on a decrease in J_{sc}, which is affected by the surface potential of HELs. By controlling the surface morphology of the HEL films with the addition of PFT-D, changes in the surface potential can be minimized, and the long-term stability of the OSCs can be improved.

CONCLUSION

In this study, the PCE and long-term stability of OSC devices were improved by adding the conjugated polymer electrolyte PFT-D to PEDOT:PSS. PFT-D reduced the acidity of the HEL solution by acting as a conjugate base of PSS. It also improved the conductivity of the HEL films by causing the aggregation of PEDOT chains by screening the Coulombic attraction between PEDOT and PSS. Also, the surface morphology and surface potential of the HELs could be controlled by adding PFT-D. The effect of the surrounding environment on the surface morphology and surface potential of the HELs with PFT-D added was reduced as compared to that of the pristine PEDOT:PSS film. It was confirmed that the improved stability of the surface morphology and potential of the HEL films had a significant effect on the long-term stability of the fabricated OSC devices. As a result, the maximum PCE of the OSCs was 8.2%, and the half-life of the devices was enhanced more than five times as compared to the device with a pristine PEDOT:PSS HEL. Although the device with PEDOT:PSS with 0.6 wt % PFT-D added showed slightly lower PCE than with 0.4 wt % PFT-D added, its long-term stability increases its usefulness. It is expected that the results of this study will

DOI: 10.1021/acsami.6b09846
ACS Appl. Mater. Interfaces 2016, 8, 31791−31798

contribute to the production of OSC devices with improved performance and lifetimes via a continuous printing process.

■ ASSOCIATED CONTENT

Supporting Information

The Supporting Information is available free of charge on the ACS Publications website at DOI: 10.1021/acsami.6b09846.

The optical properties, PL quenching data, morphology and phase images, conductivity and electrode work function with different HELs, and $J-V$ characteristics of OSCs based on PTB7:PCBM (PDF)

■ AUTHOR INFORMATION

Corresponding Author

*Tel.: +82-2-450-3498. Fax: +82-2-444-0765. E-mail: dkmoon@konkuk.ac.kr.

Notes

The authors declare no competing financial interest.

■ ACKNOWLEDGMENTS

This research was supported by the New & Renewable Energy Core Technology Program of the Korea Institute of Energy Technology Evaluation and Planning (KETEP) grant funded by the Ministry of Trade, industry & Energy (MI, Korea) (No. 20133030000180) and New & Renewable Energy Core Technology Program of the Korea Institute of Energy Technology Evaluation and Planning (KETEP), grant financial resource from the Ministry of Trade, Industry & Energy, Republic of Korea (No. 20153010140030).

■ REFERENCES

(1) Choi, M.-H.; Kim, H. Y.; Lee, E. J.; Kyung Moon, D. Control of Molecular Curvature and Crystallinity of Quinacridone-Benzoxadiazole Copolymers Using Different π Bridge for Polymer Solar Cells. *Polymer* **2016**, *91*, 162−173.

(2) O'Connor, T. F.; Zaretski, A. V.; Savagatrup, S.; Printz, A. D.; Wilkes, C. D.; Diaz, M. I.; Sawyer, E. J.; Lipomi, D. J. Wearable Organic Solar Cells with High Cyclic Bending Stability: Materials Selection Criteria. *Sol. Energy Mater. Sol. Cells* **2016**, *144*, 438−444.

(3) You, J.; Dou, L.; Yoshimura, K.; Kato, T.; Ohya, K.; Moriarty, T.; Emery, K.; Chen, C.-C.; Gao, J.; Li, G.; Yang, Y. A Polymer Tandem Solar Cell with 10.6% Power Conversion Efficiency. *Nat. Commun.* **2013**, *4*, 1446.

(4) Chen, J.-D.; Cui, C.; Li, Y.-Q.; Zhou, L.; Ou, Q.-D.; Li, C.; Li, Y.; Tang, J.-X. Single-Junction Polymer Solar Cells Exceeding 10% Power Conversion Efficiency. *Adv. Mater.* **2015**, *27* (6), 1035−1041.

(5) Han, J. P.; Lee, E. J.; Han, Y. W.; Lee, T. H.; Moon, D. K. Enhancement in Performance of Polymer Solar Cells by Introducing Solution-Processed Dipole Interlayer. *J. Ind. Eng. Chem.* **2016**, *36*, 44−48.

(6) Søndergaard, R.; Hösel, M.; Angmo, D.; Larsen-Olsen, T. T.; Krebs, F. C. Roll-to-Roll Fabrication of Polymer Solar Cells. *Mater. Today* **2012**, *15* (1−2), 36−49.

(7) Qiu, W.; Müller, R.; Voroshazi, E.; Conings, B.; Carleer, R.; Boyen, H.-G.; Turbiez, M.; Froyen, L.; Heremans, P.; Hadipour, A. Nafion-Modified MoOx as Effective Room-Temperature Hole Injection Layer for Stable, High-Performance Inverted Organic Solar Cells. *ACS Appl. Mater. Interfaces* **2015**, *7* (6), 3581−3589.

(8) Wang, F.; Tan, Z.; Li, Y. Solution-Processable Metal Oxides/chelates as Electrode Buffer Layers for Efficient and Stable Polymer Solar Cells. *Energy Environ. Sci.* **2015**, *8* (4), 1059−1091.

(9) Tan, Z.; Li, S.; Wang, F.; Qian, D.; Lin, J.; Hou, J.; Li, Y. High Performance Polymer Solar Cells with as-Prepared Zirconium Acetylacetonate Film as Cathode Buffer Layer. *Sci. Rep.* **2014**, *4*, 1474−1476.

(10) Qiu, M.; Zhu, D.; Bao, X.; Wang, J.; Wang, X.; Yang, R. WO 3 with Surface Oxygen Vacancies as an Anode Buffer Layer for High Performance Polymer Solar Cells. *J. Mater. Chem. A* **2016**, *4* (3), 894−900.

(11) Kang, T.-W.; Noh, Y.-J.; Kim, S.-S.; Joh, H.-I.; Na, S.-I. Efficient Inverted-Structure Polymer Solar Cells with Reduced Graphene Oxide for Anode Modification. *J. Ind. Eng. Chem.* **2015**, *24*, 206−210.

(12) Yang, L.; Xu, H.; Tian, H.; Yin, S.; Zhang, F. Effect of Cathode Buffer Layer on the Stability of Polymer Bulk Heterojunction Solar Cells. *Sol. Energy Mater. Sol. Cells* **2010**, *94* (10), 1831−1834.

(13) He, Z.; Zhong, C.; Huang, X.; Wong, W.-Y.; Wu, H.; Chen, L.; Su, S.; Cao, Y. Simultaneous Enhancement of Open-Circuit Voltage, Short-Circuit Current Density, and Fill Factor in Polymer Solar Cells. *Adv. Mater.* **2011**, *23* (40), 4636−4643.

(14) Song, H. J.; Lee, E. J.; Kim, D. H.; Lee, T. H.; Goh, M.; Lee, S.; Moon, D. K. Solution-Processed Interlayer of Discotic-Based Small Molecules for Organic Photovoltaic Devices: Enhancement of Both the Open-Circuit Voltage and the Fill Factor. *Dyes Pigm.* **2015**, *113*, 210−218.

(15) Song, H. J.; Lee, E. J.; Kim, D. H.; Moon, D. K.; Lee, S. Solution-Processed Interlayer of N-Type Small Molecules for Organic Photovoltaic Devices: Enhancement of the Fill Factor due to Ordered Orientation. *Sol. Energy Mater. Sol. Cells* **2015**, *141*, 232−239.

(16) Zilberberg, K.; Gharbi, H.; Behrendt, A.; Trost, S.; Riedl, T. Low-Temperature, Solution-Processed MoO $_x$ for Efficient and Stable Organic Solar Cells. *ACS Appl. Mater. Interfaces* **2012**, *4* (3), 1164−1168.

(17) Steirer, K. X.; Ndione, P. F.; Widjonarko, N. E.; Lloyd, M. T.; Meyer, J.; Ratcliff, E. L.; Kahn, A.; Armstrong, N. R.; Curtis, C. J.; Ginley, D. S.; Berry, J. J.; Olson, D. C. Enhanced Efficiency in Plastic Solar Cells via Energy Matched Solution Processed NiOx Interlayers. *Adv. Energy Mater.* **2011**, *1* (5), 813−820.

(18) Song, H. J.; Shin, G. J.; Choi, K. H.; Lee, S.; Moon, D. K. White Polymer Light Emitting Diode Materials Introducing Dendritic Quinoxaline Derivative: Synthesis, Optical and Electroluminescent Properties. *Synth. Met.* **2014**, *190*, 1−7.

(19) Vosgueritchian, M.; Lipomi, D. J.; Bao, Z. Highly Conductive and Transparent PEDOT:PSS Films with a Fluorosurfactant for Stretchable and Flexible Transparent Electrodes. *Adv. Funct. Mater.* **2012**, *22* (2), 421−428.

(20) Kim, Y.; Ryu, T. I.; Ok, K. H.; Kwak, M. G.; Park, S.; Park, N. G.; Han, C. J.; Kim, B. S.; Ko, M. J.; Son, H. J.; Kim, J. W. Inverted Layer-By-Layer Fabrication of an Ultraflexible and Transparent Ag Nanowire/Conductive Polymer Composite Electrode for Use in High-Performance Organic Solar Cells. *Adv. Funct. Mater.* **2015**, *25* (29), 4580−4589.

(21) Jeon, Y.-J.; Lee, S. S.-H.; Kang, R.; Kim, J.-E.; Yeo, J.-S.; Lee, S. S.-H.; Kim, S.-S.; Yun, J.-M.; Kim, D.-Y. Planar Heterojunction Perovskite Solar Cells with Superior Reproducibility. *Sci. Rep.* **2014**, *4*, 6953.

(22) Yook, K. S.; Lee, J. Y. Fully Flexible Organic Bistable Light-Emitting Diodes with Three Level Luminance Switching. *J. Ind. Eng. Chem.* **2015**, *23*, 179−181.

(23) Kim, H.; Park, J.; Lee, S.; Ha, C.-S.; Kim, Y. Effect of Strong Base Addition to Hole-Collecting Buffer Layer in Polymer Solar Cells. *Sol. Energy Mater. Sol. Cells* **2011**, *95* (1), 349−351.

(24) Ouyang, J. Solution-Processed PEDOT:PSS Films with Conductivities as Indium Tin Oxide through a Treatment with Mild and Weak Organic Acids. *ACS Appl. Mater. Interfaces* **2013**, *5* (24), 13082−13088.

(25) Lee, J. J.; Lee, S. H.; Kim, F. S.; Choi, H. H.; Kim, J. H. Simultaneous Enhancement of the Efficiency and Stability of Organic Solar Cells Using PEDOT:PSS Grafted with a PEGME Buffer Layer. *Org. Electron.* **2015**, *26*, 191−199.

(26) Meng, Y.; Hu, Z.; Ai, N.; Jiang, Z.; Wang, J.; Peng, J.; Cao, Y. Improving the Stability of Bulk Heterojunction Solar Cells by Incorporating pH-Neutral PEDOT:PSS as the Hole Transport Layer. *ACS Appl. Mater. Interfaces* **2014**, *6* (7), 5122−5129.

(27) Choi, M.-H.; Lee, E. J.; Han, J. P.; Moon, D. K. Solution-Processed pH-Neutral Conjugated Polyelectrolytes with One-Atom Variation (O, S, Se) as a Novel Hole-Collecting Layer in Organic Photovoltaics. *Sol. Energy Mater. Sol. Cells* **2016**, *155*, 243−252.
(28) Lee, J.-H.; Lee, B. H.; Jeong, S. Y.; Park, S. B.; Kim, G.; Lee, S. H.; Lee, K. Radical Cation-Anion Coupling-Induced Work Function Tunability in Anionic Conjugated Polyelectrolytes. *Adv. Energy Mater.* **2015**, *5* (23), 1501292.
(29) Lee, B. H.; Lee, J.-H.; Jeong, S. Y.; Park, S. B.; Lee, S. H.; Lee, K. Broad Work-Function Tunability of P-Type Conjugated Polyelectrolytes for Efficient Organic Solar Cells. *Adv. Energy Mater.* **2015**, *5* (5), 1401653.
(30) Xia, Y.; Ouyang, J. Transparent conducting polymers. In *Lecture Notes in Chemistry 91, Organic Optoelectronic Materials*; Li, Y., Ed.; Springer, 2015; Chapter 8, pp 359−392.
(31) Lim, F. J.; Ananthanarayanan, K.; Luther, J.; Ho, G. W. Influence of a Novel Fluorosurfactant Modified PEDOT:PSS Hole Transport Layer on the Performance of Inverted Organic Solar Cells. *J. Mater. Chem.* **2012**, *22*, 25057−25064.
(32) Thummalakunta, L. N. S. A.; Yong, C. H.; Ananthanarayanan, K.; Luther, J. P3HT Based Solution-Processed Pseudo Bi-Layer Organic Solar Cell with Enhanced Performance. *Org. Electron.* **2012**, *13* (10), 2008−2016.
(33) Heo, S. W.; Kim, S. H.; Lee, E. J.; Moon, D. K. Enhanced Performance in Bulk Heterojunction Solar Cells by Introducing Naphthalene Derivatives as Processing Additives. *Sol. Energy Mater. Sol. Cells* **2013**, *111* (0), 16−22.
(34) Fabiano, S.; Braun, S.; Liu, X.; Weverberghs, E.; Gerbaux, P.; Fahlman, M.; Berggren, M.; Crispin, X. Poly(ethylene Imine) Impurities Induce N-Doping Reaction in Organic (Semi)Conductors. *Adv. Mater.* **2014**, *26* (34), 6000−6006.
(35) Nardes, A. M.; Janssen, R. A. J.; Kemerink, M. A Morphological Model for the Solvent-Enhanced Conductivity of PEDOT:PSS Thin Films. *Adv. Funct. Mater.* **2008**, *18* (6), 865−871.
(36) Cruz-Cruz, I.; Reyes-Reyes, M.; Aguilar-Frutis, M. A.; Rodriguez, A. G.; López-Sandoval, R. Study of the Effect of DMSO Concentration on the Thickness of the PSS Insulating Barrier in PEDOT:PSS Thin Films. *Synth. Met.* **2010**, *160* (13−14), 1501−1506.
(37) Hou, X.; Li, Q.; Cheng, T.; Yu, L.; Wang, F.; Lin, J.; Dai, S.; Li, Y.; Tan, Z. Improvement of the Power Conversion Efficiency and Long Term Stability of Polymer Solar Cells by Incorporation of Amphiphilic Nafion Doped PEDOT-PSS as a Hole Extraction Layer. *J. Mater. Chem. A* **2015**, *3* (36), 18727−18734.
(38) Nian, L.; Zhang, W.; Zhu, N.; Liu, L.; Xie, Z.; Wu, H.; Würthner, F.; Ma, Y. Photoconductive Cathode Interlayer for Highly Efficient Inverted Polymer Solar Cells. *J. Am. Chem. Soc.* **2015**, *137* (22), 6995−6998.
(39) Lee, E. J.; Heo, S. W.; Han, Y. W.; Moon, D. K. An Organic−inorganic Hybrid Interlayer for Improved Electron Extraction in Inverted Polymer Solar Cells. *J. Mater. Chem. C* **2016**, *4*, 2463−2469.
(40) Zhao, Y.; Schwab, M. G.; Kiersnowski, A.; Pisula, W.; Baumgarten, M.; Chen, L.; Müllen, K.; Li, C. Trifluoromethyl-Functionalized Bathocuproine for Polymer Solar Cells. *J. Mater. Chem. C* **2016**, *4* (21), 4640−4646.
(41) Zhou, H.; Zhang, Y.; Seifter, J.; Collins, S. D.; Luo, C.; Bazan, G. C.; Nguyen, T.-Q.; Heeger, A. J. High-Efficiency Polymer Solar Cells Enhanced by Solvent Treatment. *Adv. Mater.* **2013**, *25* (11), 1646−1652.
(42) Lim, K.-G.; Kim, H.-B.; Jeong, J.; Kim, H.; Kim, J. Y.; Lee, T.-W. Boosting the Power Conversion Efficiency of Perovskite Solar Cells Using Self-Organized Polymeric Hole Extraction Layers with High Work Function. *Adv. Mater.* **2014**, *26* (37), 6461−6466.

DOI: 10.1021/acsami.6b09846
ACS Appl. Mater. Interfaces 2016, 8, 31791−31798